ADVANCED FUNCTIONAL MATERIALS

DOI: 10.1002/adfm.200800531

Hemoglobin-CdTe-$CaCO_3$@Polyelectrolytes 3D Architecture: Fabrication, Characterization, and Application in Biosensing**

By *Wen-Yi Cai, Liang-Dong Feng, Shan-Hu Liu,* and *Jun-Jie Zhu**

A Hemoglobin-CdTe-$CaCO_3$@polyelectrolyte 3D architecture is synthesized by a stepwise layer-by-layer method and is further used to fabricate an electrochemistry biosensor. While the calcium carbonate ($CaCO_3$) microsphere acts as an effective host for the loading of cadmium telluride (CdTe) quantum dots due to its channel-like structure, the polyelectrolyte layers further increase the loading amount and help in the formation of a thick and uniform quantum-dot ''shell'', which not only improves the stability of the spheres in water, but also contributes to the fast and effective direct electron transfer between the protein redox center and the macroscopic electrode. The materials are characterized and compared, and the possible mechanism for the direct electrochemistry phenomenon is hypothesized. Our work not only provides a facile and effective route for the preparation of quantum-dot-loaded spheres, but also sets an example of how the structure of functional materials can be tuned and related to their applications. In addition, it is one of the few examples of using $CaCO_3$ microspheres in quantum-dot loading and biosensing.

1. Introduction

The convergence of nanotechnology and biotechnology has led to a great development of the design and fabrication of functional architectures from building blocks like nanomaterials and biomolecules.[1] These assemblies often exhibit unique synergistic properties and functions and are widely used in biosensing,[2,3] drug and gene delivery,[4] biocatalysis[5] and other related areas.[6,7] Nanoparticles, especially metal and semiconductor particles, are widely used as building blocks for these assemblies due to their special electronic, photonic and catalytic properties.[8] Among them, quantum dots (QDs) have attracted intensive attention ever since their first milestone application as luminescence labels in biological detection.[9] Due to their interesting optical and electronic properties, QDs have been widely used today in both biosensing and biodiagnostic areas as versatile materials.[7,10] When QDs are conjugated with biomolecules like proteins, which are fascinating macromolecular structures in terms of their unique recognition, transport, and catalytic properties, not only can they act like as alternative labels to molecular fluorophores as fluorescence biological probes,[11] they can also function in electrochemical biosensors[2,12] or bioassays.[10] However, due to their small size, these QD-protein bioconjugates suffer from the problem of formation of QD-protein aggregates, which greatly limits their applications.[13]

An alternative and promising strategy is to utilize a biofunctionalized ''host'' labeled with QDs. Currently, three methods have been tested for the incorporation of QDs into a ''host'':[14] a) QDs are incorporated in the beads during the bead synthesis; b) QDs are trapped or affinity-partitioned directly into a preformed bead; or c) coating of the bead surface with QDs. While the problem of the first approach lies in the drawback of phase separation between the beads and QDs during the synthesis, the second method suffers from the drawback of a non-uniform distribution of QDs inside the beads.[15] The third method offers a facile and controllable means for the loading of QDs by using the layer-by-layer method. A uniform distribution of QDs was obtained when SiO_2 spheres were used as templates.[15] In another piece of work, biologically active polystyrene (PS) beads labeled with semiconductor quantum dots (QDs)with tailored QD loading were prepared via the layer-by-layer (LBL) assembly approach and applied in immunoassays.[13] However, the smooth surface and nonporous structure of the PS and the SiO_2 beads limited the loading of the QDs to a monolayer,[16] and an increase in the loading of the QDs could only be achieved by repetitive and tedious work of multilayer assembly. Recently, Nie and co-workers developed a simple strategy for the rapid and precise doping of QDs by using organically functionalized, hydrophobic, mesoporous silica beads,[17,18] yielding QD-doped beads that are 30 times brighter than nonporous PS beads of a similar size. CdTe quantum dots were also assembled on mesoporous cellular foams silicate (MCFs) and further used

[*] Prof. J.-J. Zhu, W.-Y. Cai, Dr. L.-D. Feng, S.-H. Liu
Key Lab of Analytical Chemistry for Life Science (MOE)
School of Chemistry and Chemical Engineering, Nanjing University, Nanjing, 210093 (PR China)
E-mail: jjzhu@nju.edu.cn

[**] We greatly appreciate the support of the National Natural Science Foundation of China for the Key program (20635020), Creative Research Group (20521503), and General program (20575026, 90606016). This work was also supported by the National Basic Research Program of China (2006CB933201). The authors thank Ms. Chang-Li Zhang and Professor Xiang Gao from the Model Animal Research Center of Nanjing University for their kind help.

for protein loading and biosensing.[2] A good "host" is of paramount importance for the QD loading and following applications. Porous materials seem to be promising "hosts" for this application.

Calcium carbonate, a natural mineral with great biocompatibility, has been proven to intensify enzyme performance and has been used in industry, medicine, microcapsule fabrication, and biosensing.[3] It has three anhydrous crystalline forms: calcite, aragonite and vaterite. Vaterite, the spherical polymorph of calcium carbonate, often composed of nanoparticles with diameters of 10–30 nm, has drawn more and more attention today because of its unique structure and specific features like high surface area and small specific gravity. Compared to its silica counterpart that has much-wider application today, vaterite has the advantages of easier preparation, low cost and better dispersibility in water. However, although vaterite is stable under dry conditions, when in contact with water, it transforms easily and irreversibly into a thermodynamically stable polymorph of calcite,[19] which greatly hinders its application. Another limitation lies in the lacking of a sophisticated method to functionalize its surface and make it as flexible as the silica surface.

In our previous work, we reported the fabrication of enzyme-gold nanoparticle-$CaCO_3$ bioconjugates using a two-step self-assembly process and further applied the assemblies into biosensing. The unique structure of vaterite was stabilized by the gold nanoparticles and the assembly showed improved properties due to the synergic effect of its parent materials.[3] In this work, using the stepwise layer-by-layer self-assembly process shown in Scheme 1, the vaterite structure can be stabilized with polyelectrolyte layers (PEs) (Scheme 1: step a) and further used for the loading of CdTe QDs (Scheme 1: step b). While the $CaCO_3$ microspheres offered a promising template for the loading of QDs, the polyelectrolyte layers stabilized the structure and contributed to the uniform distribution of QDs in the particles. A thick and bright QD ring pattern was observed for the CdTe-$CaCO_3$@PEs spheres in their confocal fluorescence images, indicating the presence of a QD "shell". This structure also helps in improving the stability of the hybrid material in water. The hybrid material was still porous and can be further used for the loading of hemoglobin (HB), to fabricate the HB-CdTe-$CaCO_3$@PEs 3D architecture (Scheme 1: step c). Once the bioconjugates were incorporated into a biosensor, direct electrochemistry of HB was observed and a fast and effective electron transfer between the heme center of HB and the macroscopic electrode was confirmed by electrochemistry studies. The biosensor showed good electrocatalytic performance to H_2O_2 with a linear range of $\sim 5 \times 10^{-6}$–4.5×10^{-5} mol L^{-1} and a detection limit of 2.5×10^{-6} mol L^{-1}. The small K_m of 0.77 mM indicates a high biological affinity of immobilized HB to H_2O_2. The good performance of the biosensor, as well as the effective direct electrochemistry transfer phenomenon, is the result of the synergic effect of each building block in the HB-CdTe-$CaCO_3$@PEs 3D architecture. The QD "shell" acted as a conductive "shell" tethering into the redox center of the protein and facilitated the electron-transfer process. The polyelectrolytes that help to form the "shell" indirectly contribute to the direct electrochemistry process. The $CaCO_3$ microspheres, at the same time acted like a suitable matrix that accommodated both the QDs and the HB molecules, and also offered an optimized orientation and microenvironment for the immobilized protein. Our work, as a whole, not only demonstrates that a multifunctional architecture can be assembled through a simple method, but also sets an example of the application of $CaCO_3$ microspheres as a versatile and promising material for QD loading and biosensing.

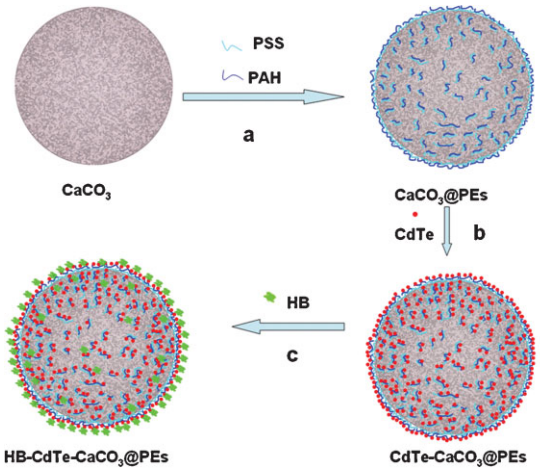

Scheme 1. Schematic illustration of the fabrication process of the HB-CdTe-$CaCO_3$@PEs 3D architecture. a) $CaCO_3$ microspheres were firstly coated with polyelectrolyte layers to produce $CaCO_3$@PEs microspheres. b) The polyelectrolyte-protected spheres were then used for the loading of CdTe quantum dots to fabricate the CdTe-$CaCO_3$@PEs hybrid material. c) In the final step, the hybrid material was used for the loading of hemoglobin (HB).

2. Results and Discussion

2.1. Assembly of Polyelectrolyte Layers onto the Surfaces of $CaCO_3$ Microspheres

Porous $CaCO_3$ microspheres, the vaterite polymorph of $CaCO_3$, is often composed of nanoparticles 10–30 nm in size and has a porous structure and channel-like interior. It has been widely used today in drug delivery,[20] protein immobilization and encapsulation,[19] biosensing[3] and polymeric-microcapsule fabrication,[21] due to this unique structure. However, the vaterite structure suffers from the problem of recrystallization when in contact with water, which could turn it into rhombohedral calcite microcrystals.

The electrostatic layer-by-layer method is widely used today to introduce polyelectrolyte layers to colloidal micro-and nanoparticle surfaces due to its simplicity and flexibility.[22] Recently, it has been found that the vaterite spheres could be stabilized by polyelectrolyte layers. In one report, poly(sodium 4-styrenesulfonate) (PSS)-stabilized $CaCO_3$ microspheres

were stored in water for six months and no obvious change in shape was observed.[20] In our experiment, the same method was used to introduce PSS/poly(allylamine hydrochloride) (PAH) thin layers onto the surfaces of $CaCO_3$ microspheres.

The layer-by-layer assembly process was monitored by microelectrophoresis measurements (expressed as a ζ-potential), which is an effective method of characterizing the surface charge of colloid particles.[23] The values of the ζ-potential of $CaCO_3$, $CaCO_3$/PSS and $CaCO_3$/PSS/PAH microspheres are shown in Figure 1. The $CaCO_3$ microspheres were positively charged at neutral pH with a ζ-potential of +11.2 mV (a in Fig. 1), which can be explained by an excess of Ca^{2+}. The carbonate ion reacts with additional H^+, whereas Ca^{2+} remains in excess with the solution absorbing on the particle surface.[19] The subsequent alternate absorption of PSS and PAH polyelectrolyte layers onto the surface yielded ζ-potentials of −14 mV (b in Fig. 1) and +16.1 mV (c in Fig. 1), respectively. In order to minimize the effect of the PEs layers on the morphology of the $CaCO_3$ spheres, only one bilayer of PEs was chosen. The positively charged $CaCO_3$@PEs spheres could be further used in the loading of CdTe QDs.

2.2. Assembly of CdTe QDs onto $CaCO_3$@PEs Microspheres

The absorption process of CdTe QDs onto the surface of $CaCO_3$@PEs was monitored by fluorescence spectroscopy. The insert in Figure 2 shows the fluorescence spectra of the as-prepared CdTe QDs (curve a) and the supernatant after CdTe absorption and centrifugation (curve b). The sharp decrease in the intensity of the emission peak at 584 nm indicates the absorption of CdTe QDs onto the surface of the $CaCO_3$@PEs microspheres. The fluorescence spectra of the $CaCO_3$ microspheres (curve c) and the CdTe-$CaCO_3$@PEs spheres (curve d) are shown in Figure 2. The salmon-pink-colored CdTe-$CaCO_3$@PEs deposit shows a strong emission at 579 nm compared to the pure $CaCO_3$ microspheres, indicating loading of the CdTe QDs. The loading amount of CdTe onto $CaCO_3$

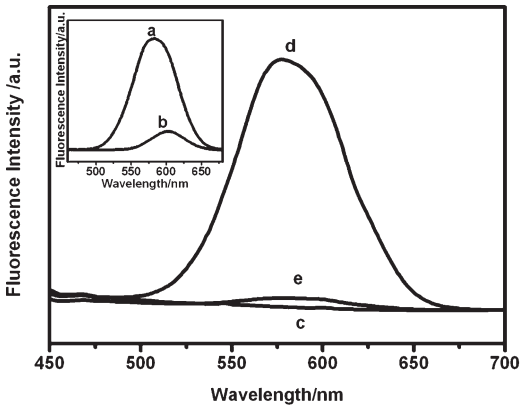

Figure 2. Fluorescence spectra of a) the as-prepared CdTe; b) the supernatant after the absorption of CdTe QDs onto the $CaCO_3$@PEs spheres; c) $CaCO_3$@PEs spheres; d) CdTe-$CaCO_3$@PEs spheres; and e) HB-CdTe-$CaCO_3$@PEs spheres.

can be calculated by the difference in intensity of the emission peak at 584 nm of the initial CdTe solution before and after loading. A rough estimate indicated that 1 mg of $CaCO_3$@PEs microspheres can accommodate 1.3×10^{18} CdTe QDs. In a control experiment, conventional mesoporous silica (MPS), $CaCO_3$ and MPS@PAH spheres were used for the loading of CdTe QDs. The loading amounts were calculated in the same way and are compared in Table 1. The loading amount of $CaCO_3$@PEs is the highest of the four samples. This indicates that the unique structure of the $CaCO_3$ microspheres and the presence of the polyelectrolyte layers both played an important part in the loading of the QDs.

The structure and surface features of the $CaCO_3$ microspheres are vital for the loading of CdTe QDs. Figure 3A shows a scanning electron microscopy (SEM) image of a polyelectrolyte-coated $CaCO_3$ microsphere. The ultrathin polyelectrolyte layers, with a thickness of around 4 nm,[24] do not affect the morphology of the $CaCO_3$ microspheres, but help to retain their spherical shape. The surfaces of the $CaCO_3$@PEs microspheres are very rough and are suitable for the loading

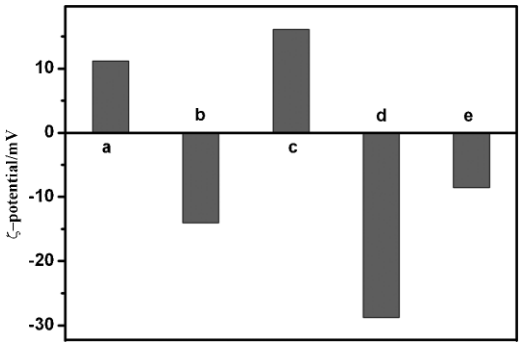

Figure 1. The values of the ζ-potentials during the whole assembly process. The bars represent a) $CaCO_3$; b) $CaCO_3$/PSS; c) $CaCO_3$@PEs; d) CdTe-$CaCO_3$@PEs; and e) HB-CdTe-$CaCO_3$@PEs microspheres.

Table 1. Comparison of the loading amounts of CdTe QDs on $CaCO_3$@PEs, $CaCO_3$, MPS/PAH and MPS microspheres. The absorption amount was calculated by the difference of the emission intensity at 584 nm between the as-prepared CdTe and the supernatant after CdTe QDs assembly.

Template	Loading amount [10^{16} CdTe per mg]
$CaCO_3$@PEs[a]	131
$CaCO_3$	88
MPS/PAH	42
MPS	8

[a] Compared with the pure $CaCO_3$ microspheres, the polyelectrolyte layers could increase the loading amount of CdTe QDs by ~49%. The loading amount on $CaCO_3$@PEs microspheres is three times that on conventional mesoporous silica spheres with PAH as the outer-most layer.

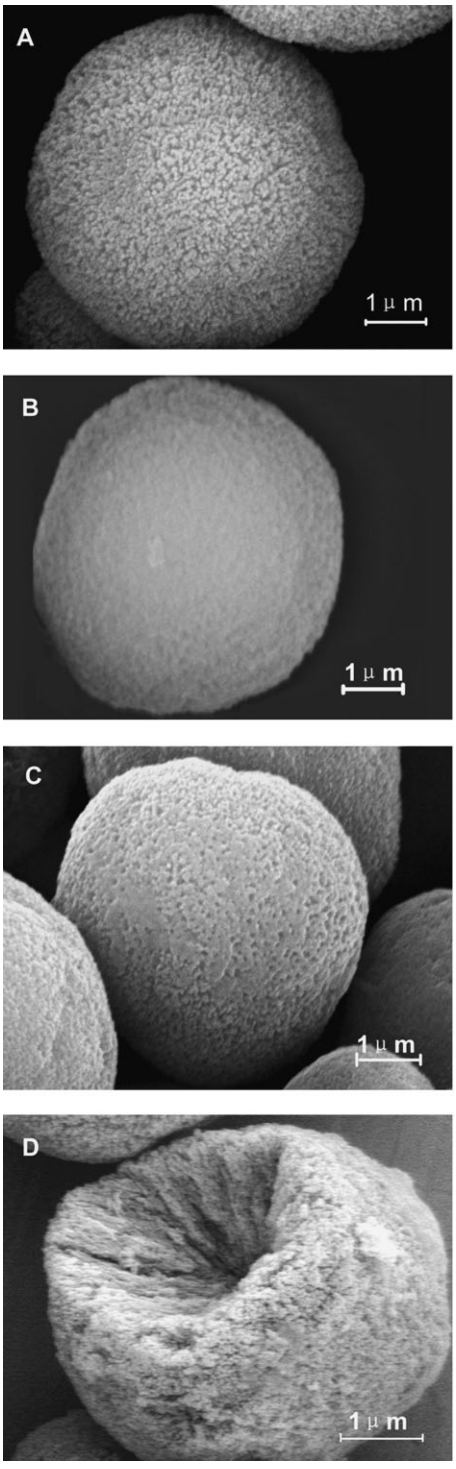

Figure 3. SEM images of A) $CaCO_3$@PEs; B) CdTe-$CaCO_3$@PEs; C) HB-CdTe-$CaCO_3$@PEs spheres; and D) a broken CdTe-$CaCO_3$@PEs sphere at higher magnification.

of CdTe QDs. The surface texture becomes smoother after the loading of the CdTe QDs, as can be observed in the SEM image of the CdTe-$CaCO_3$@PEs sphere in Figure 3B. Energy dispersive X-ray (EDX) analysis (data not shown) revealed the presence of the element Cd, which is further evidence for the presence of CdTe QDs. The spheres are still porous and this structure can be visualized at a higher magnification by field-emission scanning electron microscopy. Figure 3D shows the SEM image of a broken sphere of CdTe-$CaCO_3$@PEs, which reveals the channel like interior structure of the spheres. The channels that go directly from the outer-most surface to the center of the $CaCO_3$ microspheres are suitable for the loading of the CdTe QDs, not only onto the outside surface, but also into the interior.

The polyelectrolyte layers on the $CaCO_3$ surface are also important to the loading of QDs. First of all, they stabilize the structure of the $CaCO_3$ microspheres, so that they can be stable templates for the loading of QDs in water. They also prevent the particles from aggregating by introducing more positive charges onto the vaterite surface. $CaCO_3$@PEs microspheres were kept in water for a week and the vaterite shape was not affected. However, when $CaCO_3$ microspheres were kept in water overnight, more than 80% of the vaterite spheres were turned into the calcite polymorph.

The second role of the polyelectrolyte layers lies in their function of increasing the loading amount of CdTe QDs. Although the $CaCO_3$ microspheres alone could absorb CdTe QDs due to electrostatic interactions, using PAH as the outmost layer on the $CaCO_3$ microspheres, the absorption amount could be increased by 49% (Table 1). The ζ-potential of $CaCO_3$@PEs particles shifted from +16.1 mV to −28.8 mV, while the corresponding value of the pure $CaCO_3$ microspheres changed from +11.23 mV to −20.8 mV after the loading of CdTe QDs. The larger shift and more-negative value of the ζ-potential after the loading resulted from higher absorption amount of CdTe QDs onto the outer surface when the polyelectrolyte layers were introduced. The cationic groups ($-NH^{3+}$) of the positively charged PAH interacts so strongly with the negatively charged carboxyl ($-COO^{-}$) groups on the surface of the CdTe QDs[13] that the loading amount was greatly increased when polyelectrolyte layers were involved. Meanwhile, since the positively charged PAH also introduced more positive charges onto the surface of the $CaCO_3$ microspheres (see the value of the ζ-potentials), the enhanced electrostatic interaction between the QDs and the microspheres also contributes to the increased loading amount.

The most important function of the polyelectrolyte layers is related to the distribution of the CdTe QDs inside the microspheres. The distributions of the CdTe QDs in the $CaCO_3$@PEs and $CaCO_3$ microspheres were demonstrated using confocal laser-scanning fluorescence microscopy (CLSM), shown in Figure 4. Without the polyelectrolyte layers, the CdTe QDs distribute randomly in the $CaCO_3$ microspheres (Fig. 4A). The differences in the distribution of CdTe from particle to particle are not very obvious in the CdTe-$CaCO_3$@PEs microspheres (Fig. 4B), indicating a uniform distribution. Due to a highly effective loading of QDs, an ultrabright and thick ring pattern was observed for the CdTe-$CaCO_3$@PEs microspheres. The CdTe QD ''ring'' was directly visualized in the transmission electron microscopy

ADVANCED FUNCTIONAL MATERIALS

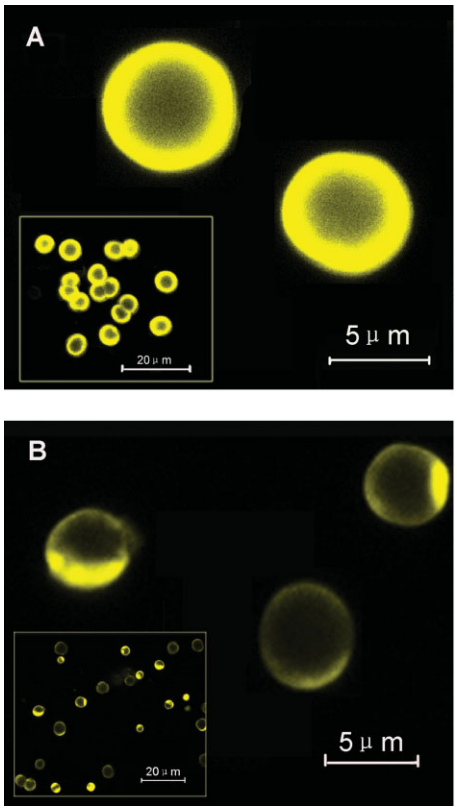

Figure 4. Confocal images of A) CdTe-$CaCO_3$ microspheres and B) CdTe-$CaCO_3$@PEs microspheres. The inserts show the overviews of the spheres.

(TEM) image of the CdTe-$CaCO_3$@PEs in Figure 5. The rough surface features and the presence of open channels in the $CaCO_3$ microspheres offer a great opportunity for QDs to load onto both the outside surface and into the open channels, resulting in a ''thick ring''. QDs could also penetrate deeply into the center of the $CaCO_3$ spheres (Fig. 4B), but most of the loaded CdTe QDs were distributed onto the outside surfaces or infiltrated into the outer-most pores and channels of the

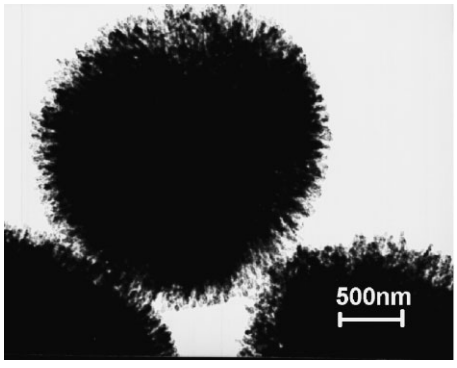

Figure 5. TEM image of CdTe-$CaCO_3$@PEs microspheres, illustrating the presence of CdTe QDs.

$CaCO_3$@PEs microspheres. Compared to a previous result for loading of dextran of different molecular weights into $CaCO_3$ microspheres,[19] it is very likely that diffusion limitation is one of the reasons that cause this kind of distribution. The pores and channels of the $CaCO_3$ microspheres could become blocked and thus prevent further infiltration of more CdTe QDs into the central area. However, an increased loading amount of QDs into the interior of the spheres can be observed for the $CaCO_3$@PEs compared to the $CaCO_3$ spheres, as shown in Figure 4. It is very likely that the infiltration and further absorption of PAH molecules into the inner surface of the microspheres increased the loading amount of QDs in the interior surface. To further investigate the distribution of the CdTe QDs in the three-dimensional CdTe-$CaCO_3$@PEs microspheres, a series of confocal images along the *z*-axis were taken and are shown in Figure 6. A ring pattern is observed for most of the optical sections collected at different levels, (Fig. 6(A-I)) perpendicular to the optical axis (the *z*-axis). However, from the center (Fig. 6A) of the microsphere to the top (Fig. 6I), the dark circle inside the ''ring'' becomes smaller and brighter, and finally disappears. This indicates that the QD ''ring'' observed in the 2D confocal image is actually a thick QD ''shell'' in the whole CdTe-$CaCO_3$@PEs microsphere. It is interesting to find that the thick QD ''shell'' contributes to enhanced stability of the structure of the composite spheres. When the $CaCO_3$@PEs particles were stored in water for more than two weeks, calcite began to form. It is probably because one bilayer of polyelectrolyte is not enough to fully cover the whole vaterite surface, thus resulting in slow recrystallization. The spherical shape of the CdTe-$CaCO_3$@PEs, in contrast, is stable in water for more than a month. This result is similar to our previous work using gold nanoparticles to stabilize the vaterite structure. The closely packed QD ''shell'' prevented the leakage of Ca^{2+} and CO_3^{2-}, thus greatly reducing the chance of recrystallization.[19] In a word, the polyelectrolyte layers help to form a uniform QD ''shell'' in the CdTe-$CaCO_3$@PEs spheres which helps in enhancing the stability of the hybrid material in water.

To further investigate the efficiency of the quantum-dos doping, conventional mesoporous silica spheres (MPS) were used for control experiments. A SEM image of the MPS beads used is shown in Figure 7A. Brunauer–Emmett–Teller (BET) data revealed surface areas of 10.4 $m^2\ g^{-1}$ and 60 $m^2\ g^{-1}$ and pore volumes of 0.093 $cm^3\ g^{-1}$ and 0.36 $cm^3\ g^{-1}$ for the $CaCO_3$ microspheres and the MPS beads, respectively. The average pore size was 33 nm for the $CaCO_3$ microspheres and 30 nm for the MPS beads. The average size of the $CaCO_3$ and MPS spheres was 5 μm as determined by SEM. As shown in Table 1, without the presence of polyelectrolyte layers, the positively charged $CaCO_3$ surface can accommodate ten times more QDs than the negatively charged MPS surface. It is obvious that QDs might have more affinity with the $CaCO_3$ surface than the silica surface. Even using PAH as the outer-most layer, the loading amount can be tripled by using $CaCO_3$ microspheres instead of MPS particles. It is quite interesting to find that the $CaCO_3$ microspheres, with a much lower surface area and pore

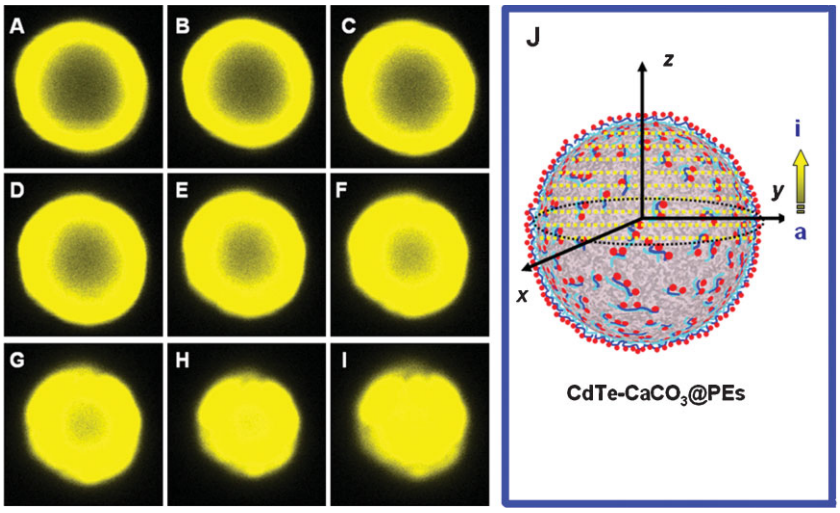

Figure 6. A–I) A series of confocal images of CdTe-$CaCO_3$@PEs microsphere taken sequentially along the *z*-axis from the center of the CdTe-$CaCO_3$@PEs sphere to the top. J) A schematic illustration of how the Z-series is taken. The yellow dashed lines (a–i) represent the levels perpendicular to the optical axis (the *z*-axis) within the microsphere.

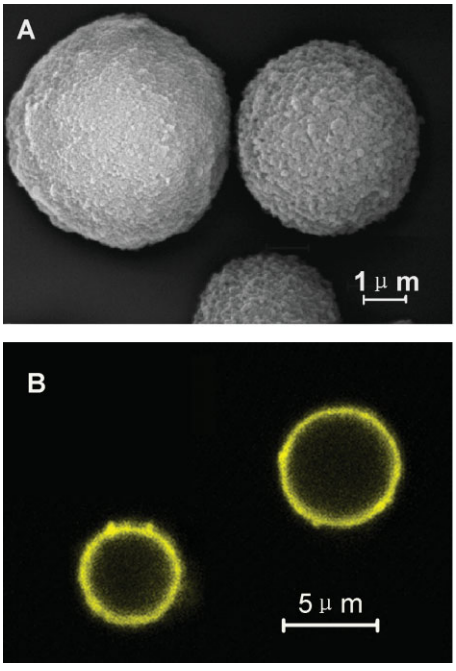

Figure 7. A) SEM image of conventional mesoporous silica (MPS) spheres used in comparison experiment. B) Confocal image of CdTe-MPS-PAH spheres.

volume, seem to be superior templates to conventional mesoporous silica beads for the loading of CdTe QDs. Figure 7B shows a confocal image of the CdTe-MPS/PAH spheres Although the mesoporous structure allows deep penetration of QDs into the central areas of the beads and the presence of the PAH layer helps to achieve a uniform distribution, a thinner and darker ring was observed compared to that of the CdTe-$CaCO_3$@PEs spheres, which comes from the lower loading amount of CdTe QDs. Compared to mesoporous silica beads, the channel-like structure of the $CaCO_3$ spheres might be more suitable for the loading of CdTe QDs, thus increasing the loading amount. Meanwhile, since it has been demonstrated that the penetration depth of QDs into PS beads does not exceed 5% of the bead radius even under extensive swelling conditions,[18] our method also demonstrates that an increased loading amount can be achieved by simply changing the template, rather than tedious and repeated work of multilayer assembly on a smooth surface.[13]

2.3. Assembly of Protein onto CdTe-$CaCO_3$@PEs Hybrid Material for Biosensing

As shown in the SEM image in Figure 3D, the CdTe-$CaCO_3$@PEs hybrid material is still porous and can be a suitable template for protein loading. With an isoelectric point (IEP) of pH 6.8, HB was positively charged at pH 6.0 in phosphate buffered saline (PBS) and can be easily assembled onto the CdTe-$CaCO_3$@PEs spheres. The bioconjugates are stable at neutral pH due to the strong interactions between the amino group of the protein and the carboxylic group of the CdTe QDs surface. The ζ-potential value changed from −28.8 mV (d in Fig. 1) to −8.57 mV (e in Fig. 1) after the loading of HB. When the negatively charged QD outer-most layer was replaced by almost-neutral protein molecules, the ζ-potential had a positive shift. A predominant change in the whole assembly process is the color change that can be observed in Figure 8A. $CaCO_3$@PEs microspheres (Fig. 8A: a) exhibit a white color, while the color of the CdTe-$CaCO_3$@PEs microspheres (Fig. 8A: b) is salmon pink. After the loading of

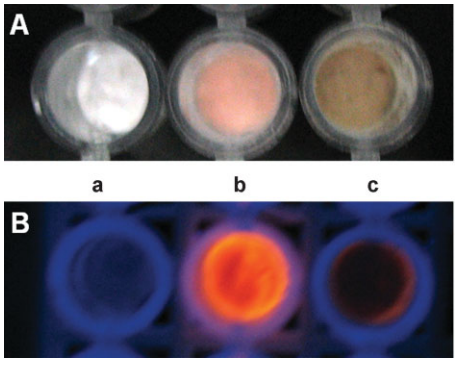

Figure 8. A) Images of a) $CaCO_3$@PEs, b) CdTe-$CaCO_3$@PEs and c) HB-CdTe-$CaCO_3$@PEs under ambient light. B) Images of a) $CaCO_3$@PEs, b) CdTe-$CaCO_3$@PEs, and c) HB-CdTe-$CaCO_3$@PEs under 260 nm UV illumination.

protein, the spheres (Fig. 8A: c) turned into dark brown. Under UV illumination (Fig. 8B), the $CaCO_3$@PEs particles (Fig. 8B: a) showed no fluorescence while the fluorescence emitted by the CdTe-$CaCO_3$@PEs (Fig. 8B: b) can be clearly observed. The fluorescence was quenched somehow after the loading of the HB and only weak fluorescence can be observed for the bioconjugates (Fig. 8B: c). This is in accordance with the results of the fluorescence spectra in Figure 2. According to a previously reported result, it is the heme center of HB that acts like an effective quencher for the fluorescence of CdTe QDs.[2] The SEM image in Figure 3C shows the surface structure of a protein-loaded sphere. It can be clearly observed that protein filled into the pores and formed aggregations on some parts of the spheres. EDX analysis (data not shown) shows an additional peak of S, compared to CdTe-$CaCO_3$@PEs spheres, and further confirmed the presence of protein. The loading amount of HB on the microspheres was calculated from UV-vis spectra before and after protein loading. It was found that around 283 μg of HB was absorbed for 1 mg of the $CaCO_3$ microspheres that were used for the preparation of the CdTe-$CaCO_3$@PEs hybrid materials.

2.4. Direct Electrochemistry of HB-CdTe-$CaCO_3$@PEs-Modified Electrodes

The quenching of the fluorescence of CdTe QDs is a very interesting phenomenon that is not only evidence for the interaction between the heme center of HB and CdTe QDs, but also renders the possibility of using the bioconjugates for biosensing. When the bioconjugates were incorporated into a biosensor, direct electron transfer of HB was observed and the feasibility of using this sensor in biosensing was evaluated.

Figure 9 shows the cyclic voltammograms (CVs) of: a) HB-CdTe-$CaCO_3$@PEs/poly(vinyl alcohol) (PVA), b) HB-$CaCO_3$@PEs/PVA, c) CdTe-$CaCO_3$@PEs/PVA, and d) HB-CdTe-MPS@PAH/PVA-modified electrodes in 0.1 M PBS (pH = 7.0) solution at 200 mV s^{-1}. CdTe-$CaCO_3$@PEs/PVA and HB-CdTe-MPS@PAH/PVA-modified electrodes exhibit no redox peaks in the potential window, indicating electroinactivity. HB-$CaCO_3$@PEs/PVA-modified electrodes exhibit one reduction peak that corresponds to the irreversible reduction of HB. Only when HB-CdTe-$CaCO_3$@PEs was used could a pair of stable redox peaks be observed. The anodic peak potential (E_{pa}) and cathodic peak potential (E_{pc}) are located at −0.342V and −0.370V (vs. saturated calomel electrode (SCE)), respectively. The small potential difference of the cathodic and anodic peak potentials of 28 mV at the scan rate of 200 mV s^{-1} indicated a fast electron-transfer process obtained for the electroactive center of the immobilized HB.[12] To further study the electron-transfer process, the effect of scan rate on the electrochemical response of immobilized HB was studied and the results are shown in Figure 10. The redox peak currents increased linearly with the increase of scan rate from 20 mV s^{-1} to 500 mV s^{-1} as can be observed in the insert, indicating a surface-controlled electrode process. According to the slope of the I_p–ν curve and following Equation (1) below, where I_p stands for the peak current n is the number of electrons, F is the Faraday constant, A is the surface area, ν is the scan rate, and T is the temperature, the average surface coverage (Γ) of HB on the surface of the modified glassy carbon electrode (GCE) was estimated to be 1.5×10^{-10} mol cm^{-2}, which was eight times that of a monolayer coverage (1.89×10^{-11} mol cm^{-2} for HB).[25]

$$I_p = \frac{n^2 F^2 \nu A \Gamma}{4RT} \quad (1)$$

It is obvious that the 3D architecture increased the protein coverage on the surface, thus increasing the electrochemistry signal. The electron-transfer rate constant K_s could be calculated according to Equation (2) when the peak-to-peak separation was less than 200 mV.

$$K_s = \frac{mnF\nu}{RT} \quad (2)$$

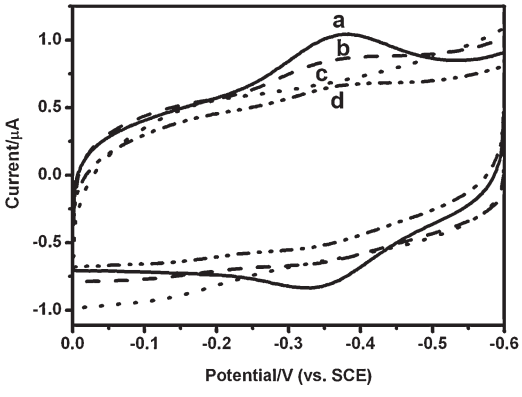

Figure 9. Cyclic voltammograms of a) HB-CdTe-$CaCO_3$@PEs/PVA, b) HB-$CaCO_3$@PEs/PVA, c) CdTe-$CaCO_3$@PEs/PVA, and d) HB-CdTe-MPS@PAH/PVA-modified glassy carbon electrode (GCE) in 0.1 M PBS at pH = 7.0 and a scan rate of 200 mV s^{-1}.

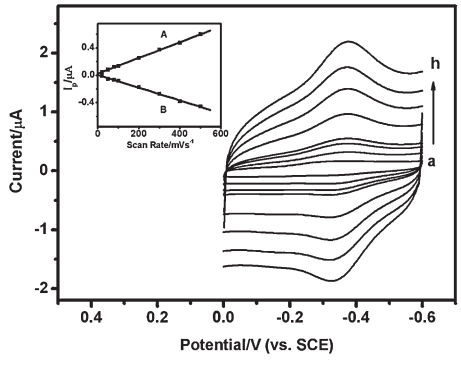

Figure 10. Cyclic voltammograms of HB-CdTe-$CaCO_3$@PEs/PVA-modified GCE in 0.1 M PBS at pH = 7.0 and at different scan rates. The scan rate from the inner to the outer curves were: a) 20, b) 50, c) 80, d) 100, e) 200, f) 300, g) 400, and h) 500 mV s^{-1}. The insert shows the plot of A) the anodic and B) the cathodic peak currents vs. scan rate.

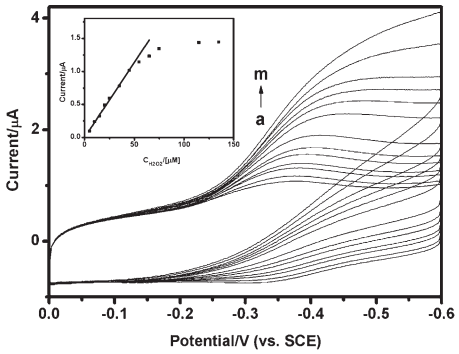

Figure 11. Cyclic voltammograms of HB-CdTe-$CaCO_3$@PEs/PVA-modified GCEs in 0.1 M PBS at pH = 7.0 in the presence of: a) 0, b) 5, c) 10, d) 15, e) 20, f) 25, g) 35, h) 45, i) 55, j) 65, k) 75, l) 135, and m) 205 μM H_2O_2 at a scan rate of 200 mV s^{-1}. The insert shows the calibration curve.

In Equation (2), m is a parameter related to the peak-to-peak separation, T is the temperature, n is the number of electrons, and v is the scan rate. The K_s value was estimated to be 10.36 s^{-1}. It was much larger than that for HB immobilized on $CaCO_3$ nanoparticles,[26] indicating a much-faster electron-transfer process.

In order to investigate the electrocatalytic activity of HB of the HB-CdTe-$CaCO_3$@PEs/PVA-modified electrode, the electrocatalytic reduction of H_2O_2 was tested by CV, as shown in Figure 11. With the increase of the concentration of the H_2O_2 in the solution, the reduction peak at about −0.37 V was enhanced (curves b–m) corresponding to the decrease of the oxidation peak. The increase of the reduction current in the reaction is because HB-Fe(II) can be oxidized with H_2O_2 and transferred to HB-Fe(III) quickly when HB-Fe(III)is directly electrochemically reduced to HB-Fe(II).[25] The calibration curve is shown in the insert of Figure 11. The biosensor's response is linear with the concentration of H_2O_2 from $\sim 5 \times 10^{-6}$–4.5×10^{-5} mol L^{-1}, and the detection limit is 2.5×10^{-6} mol L^{-1} based on a signal to noise ration (S/N) of 3. The kinetic parameter, the Michaelis constant K_m, could be readily derived from the Lineweaver-Burke Equation:[27]

$$\frac{1}{I_{ss}} = \frac{K_m}{I_{max}} \times \frac{1}{C} + \frac{1}{I_{max}} \quad (3)$$

The apparent K_m is 0.77 mM which is even smaller than previously reported results for HB/gold-nanoparticle-doped SBA,[27] which is a type of mesoporous silica, indicating a high biological affinity of the immobilized HB to H_2O_2. Six protein electrodes made at the same electrode independently showed an acceptable reproducibility with a relative standard deviation of 3% for the current determined at 20 μM H_2O_2, indicating reproducibility of the biosensor. The electrode was stored at 4 °C when not in use. No obvious decrease in the response of H_2O_2 was observed after one month of storage, indicating the stability of the biosensor.

The good performance of the biosensor is evidence for the feasibility of applying the HB-CdTe-$CaCO_3$@PEs 3D architecture in biosensing. While the comparison of the CVs of different kinds of modified electrode and the influence of the scan rate on the biosensor demonstrates a fast and effective direct electron transfer between the protein redox center and the electrode, the detection of H_2O_2 further improved the high catalytic activity of the immobilized HB. It is obvious that each building block in the HB-CdTe-$CaCO_3$@PEs 3D architecture is indispensable for the direct electrochemistry phenomenon and the sensing. A possible mechanism for the electron-transfer process is illustrated in Scheme 2. The CdTe quantum dot is of vital importance to the electron transfer between the protein and the electrode. Due to their small dimensions, which are similar to protein molecules, QDs are structurally compatible to HB molecules, thus resulting in effective interaction between the redox center of the HB and the CdTe QDs. The quenching of fluorescence of the CdTe QDs is evidence for the interaction between the CdTe QDs and the heme center of the HB molecules. The interaction is illustrated in Scheme 2C, where a and c represent respectively the conduction and valence bands for the CdTe QDs and b represents the energy band of the heme center of the HB.

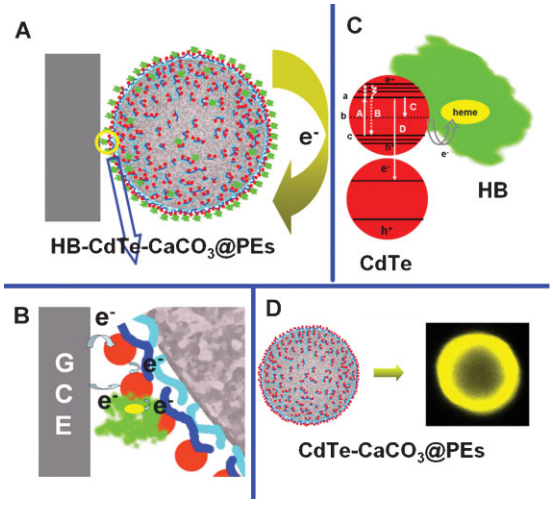

Scheme 2. Schematic illustration of the mechanism of the direct electron-transfer process. Scheme 2A illustrates the electron transfer of the HB-CdTe-$CaCO_3$@PEs bioconjugates with the electrode. The QD shell can be treated as a conductive shell that tethers into the protein redox center while connecting the electrode. Scheme 2B is a magnification that indicates two possible electron-transfer modes, directly and indirectly between one QD to the protein redox center. In Scheme 2C, a and c represent respectively the conductive and valence bands for the quantum dot, and b represents the energy band for the heme center of the HB. The white arrows represent: A) photonic emission of electrons from the CdTe valence band to conductive band, resulting in the formation of pairs of electrons (e^-) and holes (h^+); B) electron-hole combination resulting in the fluorescence of the CdTe QDs; C) electron transfer between the QDs and the heme center of the HB, resulting in fluorescence quenching; D) electron transfer from one quantum dot to the other. Scheme 2D illustrates the CdTe-$CaCO_3$@PEs hybrid material and the QD ring in a confocal-microscopy image as evidence for the QDs shell.

ADVANCED FUNCTIONAL MATERIALS

When CdTe QDs are optically excited (Scheme 2C: A), static electrons (electrons located in the valence band) become mobile (electrons located in the conduction band) within the semiconductor matrix, leaving behind them holes in the valence band.[10] The electron-hole recombination (Scheme 2C: B) causes the CdTe QDs to emit photons, and fluorescence can be observed. However, after the loading of the HB, due to electron transfer[28] (the interaction between the HB and the CdTe QDs might also come from energy transfer,[28,29] but we take electron transfer to better illustrate the whole process) between the HB and the CdTe QDs (Scheme 2C: C), the electron-hole recombination was halted, resulting in the quenching of the fluorescence of the CdTe QDs. When an electrode was involved, electrons could firstly be transferred from the electrode to the CdTe QDs and then to the heme center of the HB as shown in Scheme 2B, resulting in the direct electrochemistry phenomenon of the HB on the bioconjugates-modified electrode. The CdTe QDs act like electronic wires or nanoelectrodes between the macroscopic electrode and the redox center of the protein[8] and help to produce the direct electrochemistry phenomenon. Meanwhile, since the thick QD "shell" of the CdTe-$CaCO_3$@PEs sphere (Scheme 2D) renders the possibility of electron transfer from one CdTe QD to the other (Scheme 2C: D), it is also likely that the electron can be transferred among the CdTe QDs and finally reach the redox center of the protein (Scheme 2B). In fact, the QD "shell" can be treated as a conductive shell with mobile electrons, and the HB-CdTe-$CaCO_3$@PEs bioconjugates can be treated as a model of a group of protein molecules immobilized on a shell that tethers into their redox center and connects the electrode at the same time (Scheme 2A). Due to the effective electron transfer between the conductive shell and the redox center of the protein, a fast and effective direct electrochemistry phenomenon was achieved for the bioconjugates-modified electrode. In this case, the polyelectrolyte layers, which help to form the QD "shells", indirectly contribute to the performance of the biosensor. Finally, the $CaCO_3$ microspheres, which act like a matrix that accommodates both the CdTe QDs and the HB molecules, are an indispensable element for the direct electrochemistry of the 3D architecture. When the $CaCO_3$ microspheres were replaced with mesoporous silica templates, no direct electrochemistry phenomenon was observed. This is strong evidence for the important function of the $CaCO_3$ microspheres in the direct electrochemistry transfer process. On one hand, an increased loading amount of the CdTe QDs can be achieved due to their channel-like structure, thus increasing the efficiency of the electron-transfer process. On the other hand, it is very likely that the microspheres help to provide an optimal orientation of the HB, thus promoting the direct electrochemistry of the HB on the electrode.[27] In a word, it is the synergic effect of the HB molecules, CdTe quantum dots, polyelectrolyte layers and $CaCO_3$ microspheres that results in the fast and effective direct electron transfer between the redox center of the HB and the macroscopic electrode, as well as the good performance of the biosensor.

3. Conclusions

In this paper, the HB-CdTe-$CaCO_3$@PEs 3D architecture was fabricated through a layer-by-layer method. While the rough surface features and channel-like structure of the $CaCO_3$ microspheres offer an ideal template for quantum-dot loading, the polyelectrolyte layers contribute to the formation of a uniform distribution of CdTe QDs inside the microspheres. The thick and bright CdTe QD "shell" of the CdTe-$CaCO_3$@PEs not only enhanced the stability of the hybrid material, but also helped to realize a fast and effective direct electron transfer between the heme center of the HB molecules and the macroscopic electrode. The biosensor showed good affinity with H_2O_2 due to the synergic effect of each building block in the HB-CdTe-$CaCO_3$@PEs 3D architecture. Our work offers a model to study how the structure of functional materials can be tuned and related to their applications. The CdTe-$CaCO_3$@PEs hybrid material, with an interesting structure and unique features, is a promising material for both electronic and optical applications. While the electrochemistry application is demonstrated in this paper, the optical application of the CdTe-$CaCO_3$@PEs hybrid material is currently under investigation in our lab.

4. Experimental

Materials: HB (hemoglobin) was obtained from Sigma and was used without further purification. H_2O_2 (30% w/v solution), $CaCl_2 \cdot 2H_2O$, Na_2CO_3, KBH_4 (96%), tellurium powder (99.999%), and poly(vinyl alcohol) (PVA) (average degree of polymerization, 1800 ± 100) were purchased from Shanghai Chemical Reagent Co. (Shanghai, China). Poly(sodium 4-styrenesulfonate) (PSS) ($M_w \approx 70\,000$), poly(allylamine hydrochloride) (PAH) ($M_w \approx 15\,000$), and 3-mercaptopropionic acid (MPA) were obtained from Aldrich Chemical Co. All of the other chemicals were of analytical grade. The water used in all of the experiments was prepared in a Millipore Milli-Q purification system with a resistivity higher than 18.2 MΩ cm. Mesoporous silica (MPS) spheres with an average size of 5 μm were obtained from Lanzhou Institute of Physical Chemistry. The average pore diameter of these beads was ~30 nm. The surface area was 60 $m^2\ g^{-1}$ and pore volume was 0.36 $cm^3\ g^{-1}$.

Preparation of the $CaCO_3$ Microspheres and the CdTe QDs: The $CaCO_3$ microspheres were prepared by rapidly pouring a 0.33 M Na_2CO_3 solution into an equal volume of a 0.33 M solution of $CaCl_2$ at room temperature on a magnetic stirrer [19]. The precipitate was centrifuged, washed with MilliQ-water, and dried. Water-soluble CdTe QDs were prepared by our previous reported method [30].

Assembly of Polyelectrolyte Layers onto the $CaCO_3$ Microspheres to Prepare $CaCO_3$@PEs: Polyelectrolyte layers were assembled onto the $CaCO_3$ microspheres by the sequential deposition of the PSS polyelectrolyte and the PAH polyelectrolyte. Typically, 10 mg of $CaCO_3$ particles were suspended in 1 mL of PSS solution (5 mg mL^{-1} in 0.5 M NaCl). The suspension was sonicated for 10 min (occasionally shaking) and the excess polyelectrolyte was removed by three repeated centrifugation (4000 rpm, 5 min)/washing and redispersion cycles with water. For the subsequent assembly of positively charged PAH polyelectrolyte, 1 mL of PAH-polyelectrolyte solution (5 mg mL^{-1}, containing 0.5 M NaCl) was added.

Assembly of CdTe QDs to Fabricate CdTe-$CaCO_3$@PEs Hybrid Material: The as-prepared $CaCO_3$@PEs particles were dispersed into 2 mL of the CdTe QDs solution and sonicated for 20 min. After centrifugation, the salmon-pink-colored CdTe-$CaCO_3$@PEs hybrid

material was obtained and the supernatant was used for the analysis of the loading amount. The composites were further washed with water for three times.

Preparation of HB-CdTe-$CaCO_3$@PEs Bioconjugates: The resulting hybrid material was dispersed in 1 mL of water and an aliquot of 100 μl was added to a solution of HB (1 mg mL^{-1} in 10 mM PBS at pH = 6) and shaken for 1 h for protein absorption. The bioconjugates with a dark-brown color were then centrifuged and washed with Milli-Q water for three times. The UV-vis spectrum was used to monitor the concentration of the HB solutions before and after the assembly process. The decrease in the absorbance at 405 nm was applied to quantify the loading amount of HB immobilized onto the CdTe-$CaCO_3$@PEs particles. The bioconjugates were further washed with Milli-Q water for three times.

Fabrication of the Biosensor: A glassy carbon electrode (GCE) with diameter of 3mm was polished successively with 1.0, 0.3, and 0.05 μm alumina powder; and was rinsed thoroughly with Milli-Q water between each polishing step. Next, the polished electrode was sonicated in ethanol and Milli-Q water and was then allowed to dry at room temperature. The bioconjugates obtained were resuspended in 0.5 mL of water, and 5 μL of this suspension was deposited on the surface of the pretreated GCE. It was left to dry at room temperature. 10 μl of a 3% PVA sol (ethanol:water (v/v) = 1:1) was added for encapsulation of the bioconjugates. The electrode was then left to dry and was stored for at least 24 h at 4 °C. The biosensor was stored under the same conditions when not in use. The CdTe-$CaCO_3$@PEs/PVA-, HB-$CaCO_3$@PEs/PVA- and HB-CdTe-MPS@PAH/PVA-modified GCEs were fabricated using the same GCE by the same method except that CdTe-$CaCO_3$@PEs and HB-$CaCO_3$@PEs and HB-CdTe-MPS@PAH were used instead of the HB-CdTe-$CaCO_3$@PEs bioconjugates.

Characterization: Electrophoretic mobilities of $CaCO_3$ microparticles were measured using a Zetasizer 4 (Malvern Instruments) by taking the average of five measurements at the stationary level. The mobility u was converted to a ζ-potential using the Helmholtz-Smoluchowski relation: $\zeta = \frac{4\pi u\eta}{\varepsilon}$, where η is the viscosity of the solution and ε is the permittivity. Confocal micrographs were taken with a Leica TCS-SL confocal scanning system mounted to a Leica Aristoplan and equipped with a 40X oil-immersion objective with a numerical aperture of 1.25. The excitation wavelength was 488 nm. UV-vis spectra were recorded on a Shimadzu UV-3600 recording spectrophotometer at room temperature. The fluorescence spectra were recorded on a RF-5301 PC spectro-fluorophotometer (SHIMADZU). Brunauer–Emmett–Teller (BET) data were collected with a Micromeritics-ASAP 2020 surface-area and porosity analyzer at 77 K. The BET surface area was calculated from the linear part of the BET plot. The pore-size distribution plots were obtained by using the Barrer–Jovner–Halenda (BJH) model. Transmission electron microscopy (TEM) micrographs were recorded on a JEOL JEM 200CX transmission electron microscope, using an accelerating voltage of 200 kV. Scanning electron microscopy (SEM) measurements were carried out on an S-3000N (Hitachi, Japan) scanning electron microscope at 20 kV. Energy-dispersive X-ray (EDX) analysis was performed with an EX-250 (Horiba, Japan) attachment. Scanning electron microscopy (SEM) measurements at higher magnification were carried out on a JEOL JSM-6300F field-emission scanning electron microscope at 5 kV. Before SEM measurements were made, a double-faced adhesive paper was adhered to a stainless-steel sample desk, and the samples were uniformly scattered on another side of the paper; then the samples were gilt in an ion-sputter chamber (E-1010, Hitachi), with the pressure of the chamber less than 10 Pa. The samples were gilt for 120 s with an initial discharge current of less than 20 mA.

Amperometric cyclic-voltammetry experiments were performed using a CHI660B workstation (Shanghai Chenhua, Shanghai, China). All of the experiments were carried out using a conventional three-electrode system with the protein electrode as the working electrode, a platinum wire as the auxiliary electrode, and a saturated KCl electrode as the reference electrode. The electrolyte solutions were purged with high-purity nitrogen prior to the electrochemical experiments and blanketed with nitrogen during them.

Received: April 18, 2008
Revised: June 15, 2008
Published online: September 29, 2008

[1] E. Katz, I. Willner, *Angew. Chem. Int. Ed.* **2004**, *43*, 6042.
[2] Q. Zhang, L. Zhang, B. Liu, X. B. Lu, J. H. Li, *Biosens. Bioelectron.* **2007**, *23*, 695.
[3] W. Y. Cai, Q. Xu, X. N. Zhao, J. J. Zhu, H. Y. Chen, *Chem. Mater.* **2006**, *18*, 279.
[4] I. I. Slowing, B. G. Trwyn, S. Giri, V. S. Y. Lin, *Adv. Funct. Mater.* **2007**, *17*, 1225.
[5] S. Phadtare, A. Kumar, V. P. Vinod, C. Dash, D. V. Palaskar, M. Rao, P. G. Shukla, S. Sivaram, M. Sastry, *Chem. Mater.* **2003**, *15*, 1944.
[6] N. Kato, F. Caruso, *J. Phys. Chem. B* **2005**, *109*, 19604.
[7] J. Wang, *Electroanalysis* **2007**, *19*, 769.
[8] E. Katz, I. Willner, J. Wang, *Electroanalysis* **2004**, *16*, 19.
[9] M. Bruchez, J. M. Moronne, P. Gin, *Science* **1998**, *281*, 2013.
[10] J. M. Klostranec, W. C. W. Chan, *Adv. Mater.* **2006**, *18*, 1953.
[11] N. L. Rosi, C. A. Mirkin, *Chem. Rev.* **2005**, *105*, 1547.
[12] Q. Liu, X. B. Lu, J. Li, X. Yao, J. H. Li, *Biosens. Bioelectron.* **2007**, *22*, 3203.
[13] D. Y. Wang, A. L. Rogach, F. Caruso, *Nano Lett.* **2002**, *2*, 857.
[14] S. V. Vaidye, M. L. Gilchrist, C. Maldarelli, A. Couzis, *Anal. Chem.* **2007**, *79*, 8520.
[15] C. N. Allen, N. Lequeux, C. Chassenieux, G. Tessier, B. Dubertret, *Adv. Mater.* **2007**, *19*, 4420.
[16] N. Insin, J. B. Tracy, H. Lee, J. P. Zimmer, R. M. Westervelt, M. G. Bawendi, *ACS Nano* **2007**, *2*, 197.
[17] T. R. Sathe, A. Agrawal, S. M. Nie, *Anal. Chem.* **2006**, *78*, 5627.
[18] X. H. Gao, S. M. Nie, *J. Phys. Chem. B* **2003**, *107*, 11575.
[19] D. V. Volodkin, N. I. Larionova, G. B. Sukhorukov, *Biomacromolecules* **2004**, *5*, 1962.
[20] C. W. Wang, C. Y. He, Z. Tong, X. X. Liu, B. Y. Ren, F. Zeng, *Int. J. Pharm.* **2006**, *308*, 160.
[21] O. Kreft, A. G. Skirtach, G. B. Sukhorukov, H. Möhwald, *Adv. Mater.* **2007**, *19*, 3142.
[22] C. S. Peyratout, L. Dähne, *Angew. Chem. Int. Ed.* **2004**, *43*, 3762.
[23] D. Trau, W. J. Yang, M. Seydack, F. Caruso, N. T. Yu, R. Renneberg, *Anal. Chem.* **2002**, *74*, 5480.
[24] F. Caruro, W. Yang, D. Trau, *Langmuir* **2000**, *16*, 1485.
[25] L. Zhing, Q. Zhang, J. H. Li, *Electrochem. Commun.* **2007**, *9*, 1530.
[26] D. Shan, S. X. Wang, H. G. Xue, S. Cosnier, *Electrochem. Commun.* **2007**, *9*, 529.
[27] Y. Z. Xian, Y. Xian, L. H. Zhou, F. H. Wu, Y. Ling, L. T. Jin, *Electrochem. Commun.* **2007**, *9*, 142.
[28] R. W. Larsen, D. H. Omdal, R. Jasuja, S. L. Niu, D. M. Jameson, *J. Phys. Chem. B* **1997**, *101*, 8012.
[29] X. C. Shen, X. Y. Liou, L. P. Ye, H. Liang, Z. Y. Wang, *J. Colloid Interface Sci.* **2007**, *311*, 400.
[30] R. J. Cui, H. C. Pan, J. J. Zhu, H. Y. Chen, *Anal. Chem.* **2007**, *79*, 8494.